

# A MODEL OF THE SOLAR MAGNETIC CARPET

C. E. PARNELL

*School of Mathematics and Statistics, University of St Andrews, North Haugh, St Andrews, Fife,  
KY16 9SS, Scotland*

(Received 22 November 2000; accepted 10 January 2001)

**Abstract.** There are four key processes that dictate the behavior of the magnetic flux concentrations that form the so-called ‘magnetic carpet’ of the quiet photosphere. These processes are emergence, cancellation, coalescence, and fragmentation. Rates of emergence have been estimated from observations, but the rates of cancellation, coalescence, and fragmentation are much more difficult to determine observationally. A model is set up to simulate an area of magnetic carpet in the quiet Sun. In the model there are three imposed parameters: the rate of emergence of new flux, the distribution of emerged flux and the rate of fragmentation of flux concentrations. The rate of cancellation and the rate of coalescence are deduced from the model. From the simulations it is estimated that the average emergence rate of new flux in the quiet Sun must be between  $6 \times 10^{-6}$  and  $10^{-5}$  Mx cm $^{-2}$  s $^{-1}$  to maintain an absolute flux density of between 2.5 and 3 G. For this rate of emergence a fragmentation rate of more than  $12 \times 10^{-5}$  s $^{-1}$  is required to produce the observed exponential index for the number density of flux concentrations. This is equivalent to each fragment canceling more than once every 200 minutes. The rate of cancellation is calculated from the model and is found naturally to be equivalent to the rate of emergence. However, it is found that the frequency of cancellation is much greater than the frequency of emergence. In fact, it is likely that there are several orders of magnitude more cancellation events than emergence events. This implies that flux is injected in relatively large concentrations whereas cancellation occurs through the disappearance of many small concentrations.

## 1. Introduction

The magnetic fields that thread the surface of the Sun are very dynamic and complex in nature (Schrijver and Zwaan, 2000). There exist concentrations of magnetic flux on many scales from the large sunspots that cover more than  $2 \times 10^9$  km $^2$  and contain as much as  $10^{21}$  Mx of flux, down to the small network concentrations containing only a few times  $10^{18}$  Mx and covering just  $10^6$  km $^2$ . Even smaller concentrations have also been seen using observations taken at Big Bear Solar Observatory and reveal concentrations with just a few times  $10^{16}$  Mx of flux (Wang *et al.*, 1995). The behavior of the magnetic concentrations on all of these scales is thought to be caused by the action of at least two different processes. Sunspots are thought to emanate from the base of the solar convection zone, whilst the smaller concentrations may well originate from the bulk of the convection zone and the smallest ones from the local small-scale shear motions just below the Sun’s surface (Weiss, 1994). In this paper, we consider the concentrations at the lower end of



the scale that dominate the quiet Sun and determine what factors influence the maintenance of the magnetic fields in these regions.

The surface of the quiet Sun is dappled with positive and negative magnetic concentrations that are continuously moving and evolving, making them hard to track from birth until death. There are believed to be three types of magnetic concentration present in the quiet Sun: ephemeral regions, network fields and intra-network fields (Harvey and Martin, 1973; Harvey, Harvey, and Martin, 1975; Martin and Harvey, 1979; Harvey, 1984; Martin, 1984, 1988; Zwaan, 1987; Webb *et al.*, 1993; Schrijver and Harvey, 1994; Schrijver *et al.*, 1997). *Ephemeral regions*, defined by Harvey and Martin (1973), are clusters of bipolar pairs. Studies using data from Kitt Peak (Harvey and Harvey, 1976) and Big Bear Solar Observatory (Wang, 1988) show that ephemeral regions have a slight tendency of appearing near the edges of supergranule cells. Wang (1988) states that most (84%) ephemeral regions appear near the edges of supergranule cells compared to an estimated figure of 69% if they appeared randomly. This result is clearly counter intuitive to what one might expect, since near the edges of supergranules a downflow is expected. Martin (1988) suggests that ‘It is still an open question as to whether ephemeral regions preferentially develop either within network cells, at boundaries between two supergranules, or at the vertices of three or more cells’. Since the advent of the Michelson Doppler Imager (MDI) on SoHO (Scherrer *et al.*, 1995) the estimates for the typical sizes of supergranule cells have been revised. Hagenaar, Schrijver, and Title (1997) calculate that the typical diameters of these cells are just 14 000 km, rather than 32 000 km as previously thought (Simon and Leighton, 1964). In light of these new results for supergranule cells it is important that the birth sites of ephemeral regions are re-investigated.

The average flux of an ephemeral region is believed to be of the order of  $10^{19}$  Mx; Schrijver *et al.* (1997) estimate a mean flux of about  $1.3 \times 10^{19}$  Mx using SOHO/MDI data, but Harvey (1993) reports a slightly higher mean flux of  $3 \times 10^{19}$  Mx using data from Kitt Peak. Initially, the concentrations grow in flux as they diverge until they attain their maximum flux strength. Harvey and Martin (1973) determined that their initial separation rate is approximately  $5 \text{ km s}^{-1}$ , slowing down to about  $0.7\text{--}1.3 \text{ km s}^{-1}$  after about 30 min. Even later still, their velocity reduces to a value of about  $0.2\text{--}0.5 \text{ km s}^{-1}$ . However, Title (2000) finds that the initial separation is  $4.5 \text{ km s}^{-1}$  in the first 30 min slowing to  $1.4 \text{ km s}^{-1}$  after that. Harvey (1993) suggests that the later expansion rate of ephemeral regions is  $0.7\text{--}1.7 \text{ km s}^{-1}$ . The typical extent of a concentration within an ephemeral region is 3000–5000 km in diameter.

The second class of concentrations are *network* concentrations (Martin, 1988). These are typically found at sites of strong downflow, which are usually at the confluence of two or more supergranule cells. They typically reach flux strengths of a few times  $10^{18}\text{--}10^{19}$  Mx and have diameters of 1000 to 10 000 km. Finally, the third type of concentration is the *intranetwork* (innetwork) or intracell concentration (Livingston and Harvey, 1975; Livi, Martin, and Wang, 1985; Martin, 1984,

1988, 1990; Wang, Zirin, and Shi, 1985; Wang and Shi, 1988; Wang and Zirin, 1988; Wang *et al.*, 1995; Zirin, 1985, 1987). These are very small concentrations with fluxes of between  $10^{16}$  Mx (detection limit) and  $10^{18}$  Mx and a mean diameter of about 2000 km, although their size can vary greatly. They originate inside supergranule cells due to the emergence of (clusters of) small bipolar pairs. These concentrations are dragged along by the radial flow in the supergranules until they reach the edges of the cell. They then move along the cell edges until they interact with the surrounding network flux. They reach a peak speed of  $0.4 \text{ km s}^{-1}$  and have a r.m.s. speed of about  $0.25 \text{ km s}^{-1}$  (Wang *et al.*, 1995). The flux in these small concentrations cannot be observed well with the MDI instrument, but several studies have been carried out using data from the Big Bear Solar Observatory which can resolve flux as low as  $10^{16}$  Mx. By comparing the MDI data and the Big Bear data it appears that the bulk of the flux in the quiet photosphere is due to ephemeral regions or network fields rather than from intranetwork fields (Schrijver *et al.*, 1997).

Many detailed studies of the behavior of the magnetic concentrations on the surface of the Sun over the last 30 years have shown that there are four basic processes that occur. Firstly, *emergence*, where new magnetic concentrations appear as pairs (or clusters) of concentrations with equal flux of both polarities. On close contact initially unconnected concentrations will either *cancel* and mutually lose flux, if they are of opposite polarity (Livi, Martin, and Wang, 1985; Martin, 1984, 1988; Martin, Livi, and Wang, 1985; Martin *et al.*, 1985), or *coalesce*, if they are the same polarity. Finally, large concentrations are observed to *fragment* (split) into two (or more) different concentrations. It is not known exactly what causes the fragmentation of concentrations, but possible causes are granulation or an, as yet unknown, instability resulting in the break up of concentrations. Granulation occurs due to the overshoot of small convection cells with diameters of a thousand kilometers (Spruit, Nordlund, and Title, 1990). Since each network concentration has a diameter of, say, 5000 km as many as 25 granules may be found in each network concentration. It is likely that granulation flows continuously drive the many intense flux tubes that are believed to make up the magnetic concentrations we see in today's images causing them to follow a random walk. This means that inside every concentration the distribution of flux is continuously moved and re-organized. Unless constrained the effects of granulation will inevitably lead to the dispersion of the intense flux tubes and the break up of concentrations. Granulation is occurring everywhere at all times, but its effect is, on the whole, limited by the supergranular flows that move concentrations, and all the little intense flux tubes in them, towards regions of strong downflow. When these supergranular flows weaken, say due to a shift in the convection pattern, then granular motions can dominate and fragmentation will occur. Concentrations of all sizes can fragment, but the larger the area covered by the concentration the more likely it is to split.

Emergence of new flux into the quiet Sun is by way of concentrations providing equal amounts of positive and negative flux. It is simplest to think of these con-

centrations as being a bipolar pair, but it seems that in many cases a collection of possibly as many as ten concentrations emerge of varying flux strengths, whose total flux is zero. These clumps of newly emerged flux are known as ephemeral regions and are believed to have an average absolute flux of  $1.3 \times 10^{19}$  Mx (Schrijver *et al.*, 1997), although the estimate of this figure has varied over the years. The distribution of the emerged flux is not well known. Rates of emergence have been estimated by several authors and it is not clear what is the correct rate. Estimated rates are  $4 \times 10^{20}$  Mx hr<sup>-1</sup> (Harvey, 1993) or  $3 \times 10^{21}$  Mx hr<sup>-1</sup> (Schrijver *et al.*, 1997). These figures correspond to emergence rates of about  $1.8 \times 10^{-6}$  Mx cm<sup>-2</sup> s<sup>-1</sup> and  $1.4 \times 10^{-5}$  Mx cm<sup>-2</sup> s<sup>-1</sup>, respectively, assuming that ephemeral regions emerge uniformly over the whole solar surface.

Rates of fragmentation, coalescence and cancellation are not well known due to the difficulties in labeling and tracking individual concentrations over long periods. It is assumed though that the rate of cancellation must be approximately equal to the rate of emergence since the total absolute flux on the Sun remains approximately constant.

The dominant flow pattern on the surface of the quiet Sun is from overshoots of supergranular cells. Supergranules are estimated to have diameters between 10 000 km and 50 000 km with the latest results suggesting an average of 14 000 km (Hagenaar, Schrijver, and Title, 1997). Flows are predominantly radial in the centers of the cells and then confined along the intergranular lanes at the edges between the cells. Where three or more cells meet it is possible that a strong downflow may exist where a number of concentrations may collect. Cancellation and coalescence occur most often in the intergranular lanes and near strong downflow regions. Fragmentation can occur all over a cell, especially if the concentration covers a large area. The emergence of new flux in the form of intra network fields occurs at the centers of supergranules due to the strong convective upflows there. However, ephemeral regions appear to be able to emerge all over with a slight tendency towards emerging near the edges of supergranules.

A simple model to investigate the effects of emergence, cancellation, coalescence and fragmentation on the flux distribution within the magnetic carpet has been developed by Schrijver *et al.* (1997). They present results from a series of Monte Carlo simulations in which the rates of emergence, cancellation, coalescence and fragmentation are all prescribed and the numbers of concentrations evolve according to a suggested equation of ‘magneto-chemistry’. These simulations provide a good first handle on the effects of the four processes, but all their rates are simply dependent on time and flux and not on space.

In this paper, we discuss the development and present results from a new two-dimensional model of the magnetic carpet. In our model, cancellation and coalescence arise naturally as opposed to being prescribed as in Schrijver *et al.* (1997). This allows us to study the effect of varying the rate and distribution of emergence of flux on the absolute flux density and the distribution of flux concentrations. Also, the rate of fragmentation is an input parameter and so the effect of varying this is

studied. Since cancellation occurs naturally within the model we can estimate how the rate of cancellation varies with respect to emergence and fragmentation. The model is two dimensional and so we have the possibility of determining the rates of cancellation both spatially and temporally. However, in order to produce results that can easily be compared we average in space to produce rates that are simply dependent on time.

## 2. The Model

The model consists of a two-dimensional periodic domain in which a series of regular hexagonal supergranule cells are packed. We consider a collection of 36 ( $6 \times 6$ ) supergranule cells each with a diameter  $d$  of 14 000 km. The supergranules cover an area equal to  $13.5\sqrt{3}d^2$ , which is approximately  $4.5 \times 10^9$  km<sup>2</sup> for  $d = 14\,000$  km (i.e., it is roughly 0.07 percent of the Sun's total surface area). The area per supergranule is equivalent to  $1.25 \times 10^8$  km. The following subsections detail assumptions that are adopted in the model about the nature of the flux concentrations and their motions, as well as the processes of emergence, fragmentation, coalescence and cancellation.

### 2.1. FLUXES, AREAS AND SPEEDS OF THE MAGNETIC CONCENTRATIONS

All concentrations are assumed to be circular and to have a Gaussian profile of magnetic field across them (Figure 1(a)). The peak magnetic field,  $|B_{\max}|$ , in each concentration is assumed to be 1000 G, whereas the minimum magnetic field,  $|B_{\min}|$ , in each concentration is set at 20 G. This means that each concentration of flux,  $\phi$ , has a radius,  $r$ , equal to

$$r = \sqrt{2\sigma^2 \log(|B_{\max}|/|B_{\min}|)} = \sqrt{2\sigma^2 \log(50.0)}, \quad (1)$$

where

$$\sigma = \sqrt{\frac{|\phi|}{2\pi(|B_{\max}| - |B_{\min}|)}}.$$

Figure 1(b) shows graphically how the radius of the magnetic concentrations varies with flux,  $|\phi|$ , for concentrations with total fluxes up to  $3 \times 10^{19}$  Mx.

The speeds of observed magnetic concentrations with fluxes between  $10^{18}$  Mx and  $10^{19}$  Mx have been observed to lie in the range 0.03 to 2 km s<sup>-1</sup>. Exact speeds are hard to determine and seem to depend on the time scale with which the data is averaged. Hagenaar *et al.* (1999) investigated speeds of concentrations with respect to their flux content and found a fairly wide distribution for each of the four time intervals over which they averaged. However, by averaging the speeds in each  $10^{18}$  Mx flux interval they found the data roughly corresponded to an exponential. The speed,  $v$ , of each concentration is assumed to be proportional to the concentration's flux,  $|\phi|$ , such that

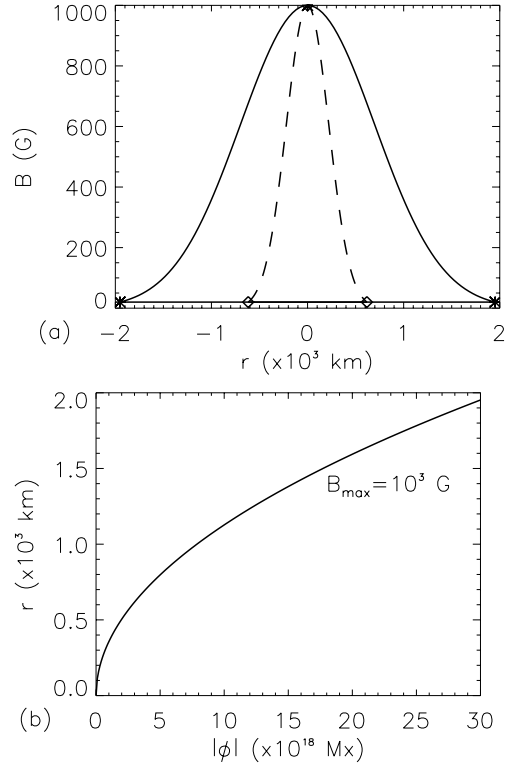


Figure 1. (a) The magnetic field profiles of concentrations with fluxes,  $|\phi|$ , of  $3 \times 10^{18}$  Mx (*dashed*) and  $3 \times 10^{19}$  Mx (*solid*). (b) Plot of concentration radii,  $r$ , versus concentration flux,  $|\phi|$ , for concentrations with  $B_{\max} = 1000$  G and  $B_{\min} = 20$  G.

$$v(\phi) = \sqrt{v_0^2 \exp(-\alpha|\phi|/\phi_0)} \quad (\text{km s}^{-1}). \quad (2)$$

Figure 2(a) shows the exponential curves that best fit the speeds averaged over time intervals of 1500 s, 3000 s, 6000 s, and 12 000 s (based on figures by Hagenaar *et al.*, 1999). The solid curve represents the best fit to the data averaged over 3000 s and has an  $\alpha$  of approximately  $-0.188$ ,  $v_0 = 0.171$ , and  $\phi_0 = 2.5 \times 10^{18}$  Mx. This is the relation that we use to estimate speeds for our concentrations.

In the model a concentration with flux,  $|\phi|$ , is assumed to move with speed,  $v(|\phi|) + W$ , where  $v(|\phi|)$  is given by Equation (2) and  $W$  is a normally distributed random number lying between  $-0.12$  and  $0.12$ . Figure 2(b) shows a plot of 30 000 randomly generated speeds to give a feel for the spread of speeds of the concentrations.

## 2.2. MOTIONS OF THE MAGNETIC CONCENTRATIONS

It is assumed that magnetic concentrations emerge in pairs of opposite polarity inside supergranule cells and that they then move about according to a series of rules

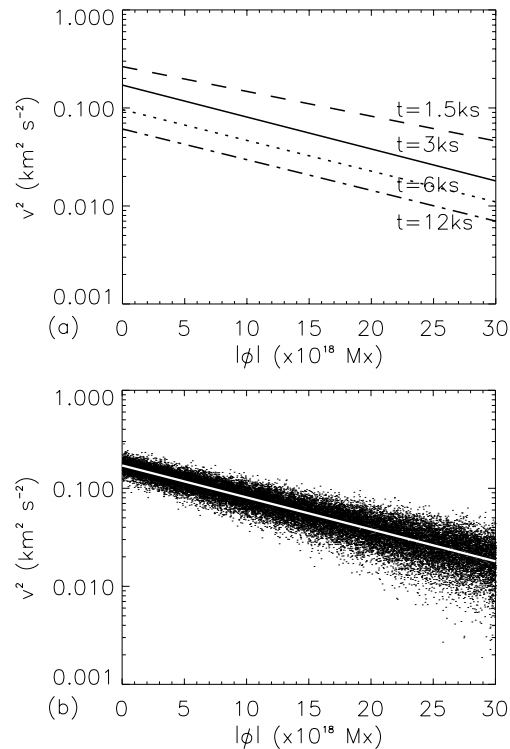


Figure 2. (a) Observed average speed profiles for data averaged over 1500 s (*dashed*), 3000 s (*solid*), 6000 s (*dotted*) and 12000 s (*dot-dashed*). (b) Plot showing a typical distribution of velocities for concentrations with fluxes between  $10^{16}$  and  $3 \times 10^{19}$  Mx.

specified below. These rules are based on the general behavior of concentrations as observed by MDI (Schrijver, 1999, private communication). Initially, when a pair of concentrations emerge they move in opposite directions approximately along a single axis. Upon reaching the edges of a supergranule cell they move along these edges, where they are confined, until they interact with another concentration. When reaching a cell edge a concentration may either

- move along the edge in the direction of any existing concentrations on the edge;
- or, if there are no concentrations already on that edge, move along the edge in either direction (randomly chosen with equal probability).

Once a concentration has reached an edge it only travels in one direction along that edge – the same direction as all other concentrations on the edge at that time. However, once an edge is empty of concentrations it no longer has a prescribed direction and so the next concentration to travel along that edge determines the direction of the edge until again the edge is empty of concentrations.

When a vertex has been reached a number of possibilities exist depending on whether the other two edges extending out from the vertex already have prescribed

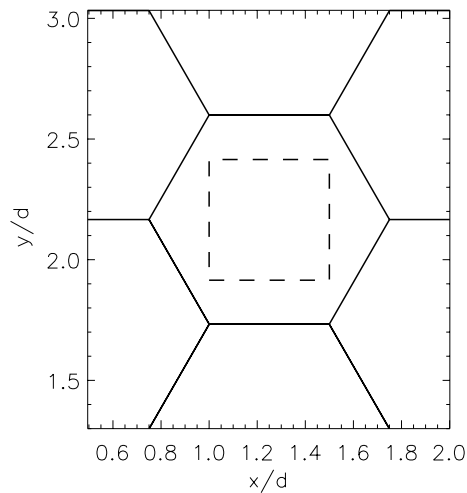


Figure 3. The dashed box outlines the region in which ephemeral regions may emerge within each supergranule cell. The axes are non-dimensionalised with respect to the diameter,  $d$ , of a supergranule.

flows along them. If an edge does not already have a prescribed direction, then one is randomly chosen and is temporarily assigned to it for the purpose of determining which way the concentration at the vertex can move.

–If both edges have flows directed away from the vertex then the concentration may either: (i) split into two concentrations of unequal size such that a portion of the original concentration travels down each of the edges, (ii) or travel as a whole down either one of the two edges.

–If both edges have flows directed towards the vertex the concentration remains stationary.

–If only one edge has a flow directed away from the vertex then the concentration travels as a whole along that edge.

### 2.3. EMERGENCE

Concentrations emerge as pairs of equal, but opposite polarity flux. They are assumed to appear randomly in any one of the supergranule cells anywhere inside a square box of length  $l = d/2$ , where  $d$  is the diameter of the supergranule, centered in the cell, such as the dashed box shown in Figure 3. The concentrations move in opposite directions away from each other along an axis which can have any orientation (chosen at random) and move with a prescribed velocity that is related to the magnitude of their flux,  $|\phi|$  (see Section 2.2). The flux with which each concentration emerges is some multiple of  $10^{16}$  Mx, i.e., concentrations are made up of integer numbers of miniature flux tubes. We have placed this minor restriction on the flux strengths of concentrations to prevent infinitesimally small flux concentrations being created by fragmentation and cancellation or numerical

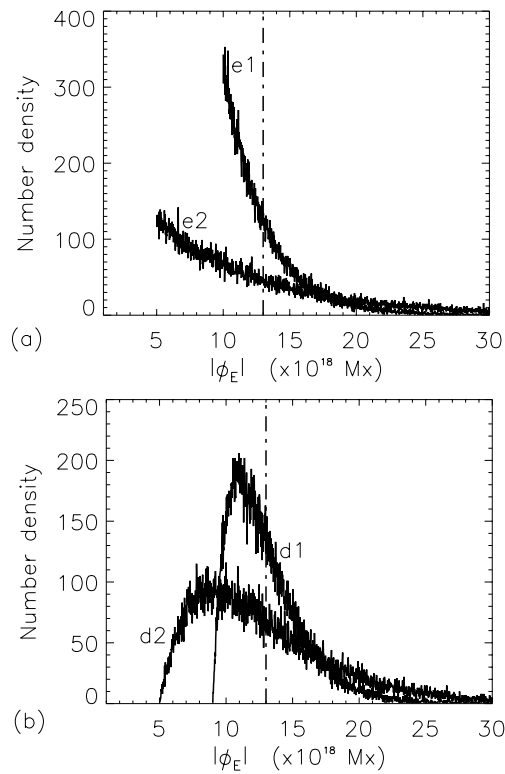


Figure 4. Distributions of emerged concentrations. Distributions  $e1$  and  $e2$  are both exponential and  $d1$  and  $d2$  are both skewed-normal. All four distributions have a mean of  $1.3 \times 10^{19}$  Mx indicated by the dot-dashed line.

rounding. This also means the numbers of concentrations in the area at any one time must be finite and cannot become excessive.

The observed total flux of newly emerged bipoles averages at  $\sim 1.3 \times 10^{19}$  Mx (Schrijver *et al.*, 1997). In our model, we therefore allow pairs of concentrations to emerge whose total flux value is chosen at random, but under the constraint that the distribution of emerged fluxes has a mean flux of  $1.3 \times 10^{19}$  Mx and is distributed in a particular manner. For instance, we have considered four emerged flux distributions,  $D_E$ , that are either exponential or skewed-normal in nature (Figure 4).  $D_E = e1$  and  $D_E = e2$  represent exponential distributions with minimum absolute fluxes of  $1 \times 10^{19}$  Mx and  $5 \times 10^{18}$  Mx, respectively. The skewed-normal distributions,  $D_E = d1$  and  $D_E = d2$  have minimum absolute fluxes  $9 \times 10^{18}$  Mx and  $5 \times 10^{18}$  Mx, respectively, and modal fluxes  $1.05 \times 10^{19}$  Mx and  $8.5 \times 10^{18}$  Mx, respectively.

The rate of emergence,  $R_E$ , is a variable parameter in the model. During our simulations we vary  $R_E$  in order to determine the most likely emergence rate that

gives the observed absolute flux density on the quiet Sun of approximately 2.5–3 G.

#### 2.4. FRAGMENTATION

Magnetic concentrations are known to fragment or split at any time. This process, known as fragmentation, is not well understood from observations and so the rate of fragmentation is also a parameter in the model. A concentration can only split into two concentrations at any one time step. The flux in these new concentrations,  $\phi_1$  and  $\phi_2$  is such that

$$\phi_1 = \phi p \quad \text{and} \quad \phi_2 = \phi(1 - p) ,$$

where  $\phi$  is the flux in the original concentration and  $p$  is a random number between 0.55 and 0.95. These new concentrations move with randomly chosen speeds appropriate to their flux content and move either in the same direction as the original concentration if on an edge of a cell, or move in slightly different directions if in the cell interior. The new directions of travel for the concentrations in the cell interior are at angles of  $\pm 0.3\pi q$  from the direction of motion of the original concentration, where  $0 < q \leq 1$  is a random number. This relationship has been chosen such that it is possible for fragmentation to occur during the expansion of the ephemeral region across the supergranule cell. However, a relatively small angle has been chosen such that the ephemeral region still basically expands along a single axis.

The rate of fragmentation is both a function of time and of flux. Firstly, it is assumed that concentrations fragment approximately once every  $T$  seconds, giving a fragmentation rate,  $R_f$ , which depends on time alone, of  $1/T \text{ s}^{-1}$ . The time at which a concentration fragments is determined randomly and is independent of the size of the time step. However, as we have already said, fragmentation depends on flux as well as time and so we have a separate rate of fragmentation that depends purely on flux. This is defined such that a concentration with flux,  $|\phi|$ , may fragment provided

$$\frac{q(\psi - \phi)}{\psi} < k_f ,$$

where  $q$  is a random number ( $k_f < q < 1.0$ ),  $\psi$  is chosen to be a number that is typically at the large end of the range of expected values for  $\phi$  and  $0 < k_f \leq 1$ . That is to say the probability that a concentration fragments increases the greater the flux in the concentration. It is possible to determine the concentrations that have zero probability of fragmentation and those that have a probability of one. Those concentrations with zero probability have a flux  $|\phi|$ , where  $|\phi| < \phi_{kl} = \psi(1 - k_f / \min(q))$ . The minimum value of  $q$  has been deliberately chosen such that  $\phi_{kl} = 0$  meaning that all concentrations can fragment (except those with one unit of flux,  $\phi = 10^{16} \text{ Mx}$ , for numerical reasons). We can also calculate which concentrations will always fragment (have a fragmentation probability of 1). These

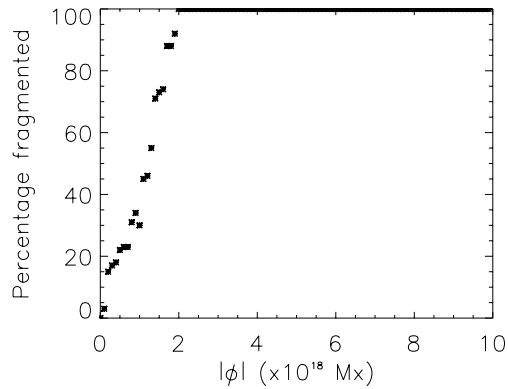


Figure 5. Percentage of concentrations with flux,  $|\phi|$ , that fragment vs  $|\phi|$ . In this case  $k_f = 0.75$  and  $\psi = 8 \times 10^{18}$  Mx.

have a flux  $|\phi|$ , where  $|\phi| > \phi_{ku} = \psi(1 - k_f / \max(q)) = \psi(1 - k_f)$ , since  $\max(q)=1$ .

Furthermore, concentrations can only fragment provided that they satisfy all the above criteria and are not in contact with any other concentrations from which they have just split or with which they have emerged. This added minor restriction on fragmentation is imposed to aid computing. If it were not imposed, steps would be needed to ensure coalescence did not occur between concentrations that had just fragmented from recently fragmented concentrations!

In the model the value of  $k_f$  is 0.75 and  $\psi$  is kept fixed at  $8 \times 10^{18}$  Mx. Therefore, in the model  $R_f$ , the fragmentation rate dependent on time, is the only parameter that varies the rate of fragmentation. This implies that all flux concentrations can fragment (except those with only one unit of flux,  $|\phi| = 10^{16}$  Mx) since  $\phi_{kl} = 0$  Mx and fragments with more than  $\phi_{ku} = 2 \times 10^{18}$  Mx will always fragment within  $1/R_f$  seconds. Given a set of fluxes in the range  $10^{16}$  to  $10^{19}$  Mx the probabilities of fragmenting in  $1/R_f$  seconds, if  $k_f = 0.75$  and  $\psi = 8 \times 10^{18}$  Mx, are plotted in Figure 5.

Figure 6(a) shows a plot of the largest fragmented concentration versus the original concentration for a uniform distribution of 10 000 concentrations so the typical spread of fragmented concentration sizes can be seen.  $k_f$  is taken to be 0.75 and  $\psi = 8 \times 10^{18}$  Mx. The distribution of these new concentrations is plotted in Figure 6(b) as a solid line and can be compared with the original uniform distribution of concentrations indicated by the dashed line.

## 2.5. COALESCENCE AND CANCELLATION

When two magnetic concentrations come into contact they will either coalesce (merge) with one another, if they are of the same polarity, or cancel, if they are of opposite polarity. In the model, coalescence and cancellation occur between

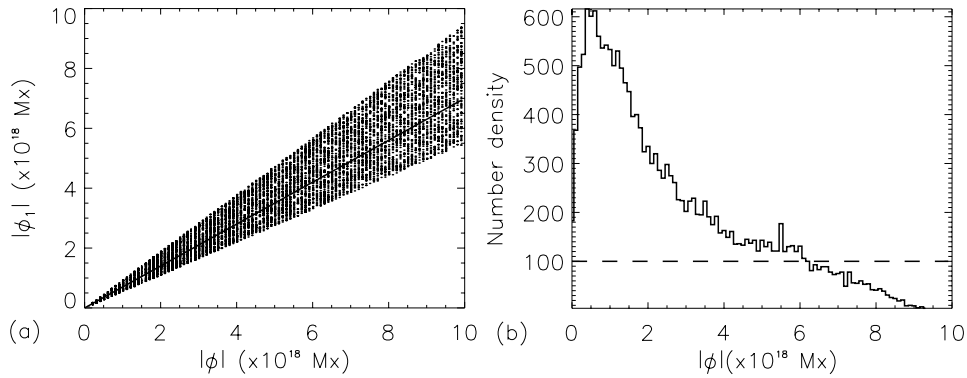


Figure 6. (a) Flux of the largest fragmented concentration is plotted versus the flux of original concentration. (b) Distribution of all fragments after fragmentation from an initial uniform distribution is shown. In both cases  $k_f = 0.75$  and  $\psi = 8 \times 10^{18}$  Mx.

two concentrations provided their centers are separated by a distance less than the radius of the larger concentration.

In coalescence the overlapping concentrations combine to form a single large concentration whose flux is equal to the sum of the original concentrations. This concentration will then move in the direction of the largest original concentration at a speed slower than either of the original concentration speeds and randomly chosen in accordance with the magnitude of its flux.

When cancellation occurs between two concentrations of opposite sign a single concentration is formed whose flux is equal to the sum of the original fluxes. This time, however, the magnitude of the new concentration's flux will be smaller than either of the two previous fluxes and so the new concentration moves faster. It will move in the direction of the original concentration with the largest flux magnitude. Clearly, it is possible that the two original concentrations may have the same magnitude of flux and so may completely cancel each other leaving no remaining small concentration.

Also, it is worth mentioning that, if three or more concentrations overlap each other simultaneously, then each of these scenarios is treated separately and they do not count as two or more two-concentration-contact situations. This is because it is not possible to tell which concentrations collided first, unless the time step is very small, and so it is not possible to pair the concentrations correctly. At most, we have come across four concentrations coming into contact at any one time, but in general we try to avoid these situations by reducing the time step of the model in an attempt to resolve such complex meetings of concentrations.

The rate of cancellation and rate of coalescence are *implicit* in the model and not determined by any one input parameter. They occur as a natural consequence of the movement of concentrations. It is, however, possible to calculate these rates, as discussed in the next section.

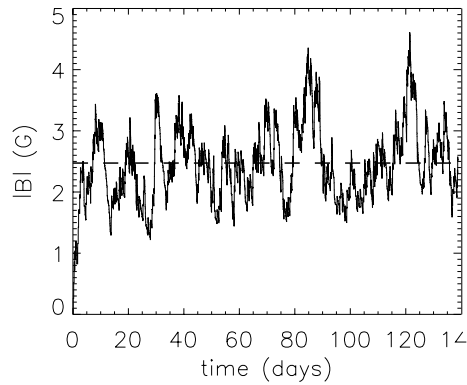


Figure 7. Plot of the absolute flux density against time for one run of the model. The *dashed line* represents the average absolute flux density,  $b$ .

### 3. Results

The model has three key parameters that can be varied and affect the absolute flux density and distribution of flux. These parameters, as discussed in the previous section, are

- $R_E$  – rate of emergence of new flux ( $\text{Mx cm}^{-2} \text{s}^{-1}$ );
- $D_E$  – distribution of newly emerged flux: exponential –  $e1$  and  $e2$  and skewed-normal –  $d1$  and  $d2$  (see Section 3.3 for details of these distributions);
- $R_f$  – rate of fragmentation ( $\text{s}^{-1}$ ).

In the following four sections, we consider the effects of these parameters and determine limits for them on the quiet Sun.

#### 3.1. ABSOLUTE FLUX DENSITY

In quiet regions of the Sun the average absolute flux density is approximately 2.5 G to 3 G (Schrijver *et al.*, 1997). This is the first and possibly the most important constraint on our model.

To calculate the absolute flux density, we run the model for a particular set of input parameters for a period of 40 000 time steps which equates to 140 days with a time step of 5 min. This number of time steps was chosen such that the model ran long enough to determine if the flux density really oscillated around some average value and ensured that we had plenty of results from the runs to allow us to do reasonable statistics. We initially assume that there is no flux in the box and emergence is at the chosen rate and with the chosen distribution. In all cases, after about 20–30 days the absolute flux density stops growing and begins to oscillate about an average flux density  $b$  (Figure 7). The amplitude of the oscillations about this average can be as much as  $\pm 2$  G. Since the model requires many random number generations, different average flux densities,  $b$ , are obtained for runs with the same input parameters, but different seeds. Therefore, to determine the mean

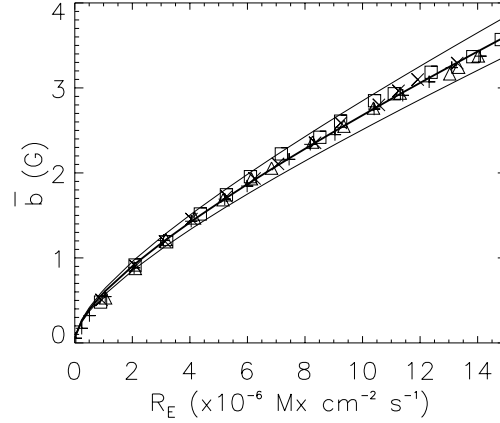


Figure 8. Absolute flux density versus emergence rate,  $R_E$ , for emerged flux distributions,  $D_E$ , equal to  $e1$  ( $\Delta$ ),  $e2$  ( $\square$ ),  $d1$  ( $+$ ), and  $d2$  ( $\times$ ). The rate of fragmentation,  $R_f$ , is held fixed at  $4.2 \times 10^{-5} \text{ s}^{-1}$ , which is equivalent to one fragmentation every 400 min per concentration. The curve of best fit is indicated by a thick curve whilst the thin curves represent the fits given by twice the standard error.

flux density for a particular set of input parameters the mean  $b$  from ten runs, each with a different seed, is calculated to give a single value,  $\bar{b}$ , for the absolute flux density.

In Figure 8, the absolute average flux density,  $\bar{b}$ , is plotted against the emergence rate,  $R_E$ , for the four different emerging flux distributions,  $e1$  ( $\Delta$ ),  $e2$  ( $\square$ ),  $d1$  ( $+$ ), and  $d2$  ( $\times$ ). The fragmentation rate,  $R_f$ , is held fixed at  $4.2 \times 10^{-5} \text{ s}^{-1}$  and is equivalent to one fragmentation every 400 min per concentration. On this plot it is not easy to distinguish the individual symbols since they often appear on top of each other clearly demonstrating that the results from all four distributions are very similar. They all show the same increase in  $\bar{b}$  from 0.5 G to about 4 G for an increase of  $R_E$  from  $1.0 \times 10^{-6} \text{ Mx cm}^{-2} \text{ s}^{-1}$  to  $15.0 \times 10^{-6} \text{ Mx cm}^{-2} \text{ s}^{-1}$ . Three extra points for the flux distribution  $d1$  ( $+$ ) are plotted for values of  $R_E$  equal to  $0.05 \times 10^{-6}$ ,  $0.26 \times 10^{-6}$  and  $0.52 \times 10^{-6}$  to confirm that the data really do curve towards the origin as might be expected. A curve of the form

$$\bar{b} = a_0 \sqrt{R_E} + a_1 R_E \quad (3)$$

is fitted to the data and is indicated on Figure 8 by a thick curve. The parameters  $a_i$  that give the best fit are

$$a_0 = 470.1 \pm 24.8 \quad \text{and} \quad a_1 = (1.19 \pm 0.09) \times 10^5,$$

where the errors quoted are twice the standard error. The two thin curves on the graph represent the fits given by twice the standard error of the parameters  $a_i$ . The curve goes through the origin, since of course  $\bar{b} = 0$  if no flux is injected.

In Figure 9, the absolute average flux density,  $\bar{b}$ , is plotted against the fragmentation rate,  $R_f$  for all the emerging flux distributions. Here the emergence rate,  $R_E$ ,

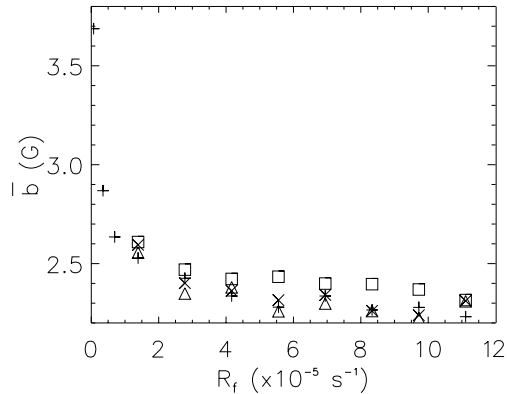


Figure 9. Absolute flux density versus rate of fragmentation,  $R_f$ , for emerged flux distributions,  $D_E$  equal to  $e1$  ( $\Delta$ ),  $e2$  ( $\square$ ),  $d1$  (+), and  $d2$  ( $\times$ ). The emergence rate,  $R_E$ , is held fixed at  $8.3 \times 10^{-6} \text{ Mx cm}^{-2} \text{ s}^{-1}$ .

is held fixed at  $8.3 \times 10^{-6} \text{ Mx cm}^{-2} \text{ s}^{-1}$ . Again, all the graphs vary in roughly the same way, but the effect of  $R_f$  is much weaker than that of  $R_E$  with  $\bar{b}$  lying in the range 2.2 G to 2.7 G, whilst  $R_f$  varies between  $1.4 \times 10^{-5} \text{ s}^{-1}$  and  $1.1 \times 10^{-4} \text{ s}^{-1}$  (equivalent to one fragmentation every 20 hours or 2.5 hours, respectively.)

These results indicate that the dominant effect on the absolute flux density comes from the emergence rate. The distribution of the emerged flux seems to have very little effect at all, whereas, the effect of fragmentation is also weak for fragmentation rates,  $R_f$ , of  $2.7 \times 10^{-5} \text{ s}^{-1}$ , equivalent to one fragmentation per 10 hours, or faster. However, fragmentation rates,  $R_f$ , of less than this value, lead to a more dramatic rise in absolute flux as shown by the extra + points for the  $d1$  emergence distribution plotted for  $R_f$  equal to  $0.07 \times 10^{-5}$ ,  $0.35 \times 10^{-5}$ , and  $0.70 \times 10^{-5} \text{ s}^{-1}$  equivalent to approximately one fragmentation every 400, 80, and 40 hours, respectively. This is because, with so little fragmentation, the flux concentrations will be large and therefore slow moving, with relatively few of them being present; thus, they rarely interact and cancel. Increasing the rate of fragmentation has the inverse effect and creates many small flux concentrations which frequently interact. However, each interaction can mean either a cancellation or a coalescence and so for greater  $R_f$  the curve tends to a constant absolute flux density,  $\bar{b}$ . Furthermore, assuming that the observed absolute total flux density lies between 2.5 G and 3 G, the emergence rate is likely to be in the range  $6.0 \times 10^{-6} \text{ Mx cm}^{-2} \text{ s}^{-1}$  to  $10.0 \times 10^{-6} \text{ Mx cm}^{-2} \text{ s}^{-1}$ , which lies comfortably within the observed rates of emergence given by Schrijver *et al.* (1997) and Harvey (1993) of  $1.8 \times 10^{-6} \text{ Mx cm}^{-2} \text{ s}^{-1}$  and  $14.0 \times 10^{-6} \text{ Mx cm}^{-2} \text{ s}^{-1}$ , respectively.

### 3.2. FLUX DISTRIBUTION

The distribution of flux concentrations is also important and can be compared with observations. Schrijver *et al.* (1997) determined that the flux distribution from a

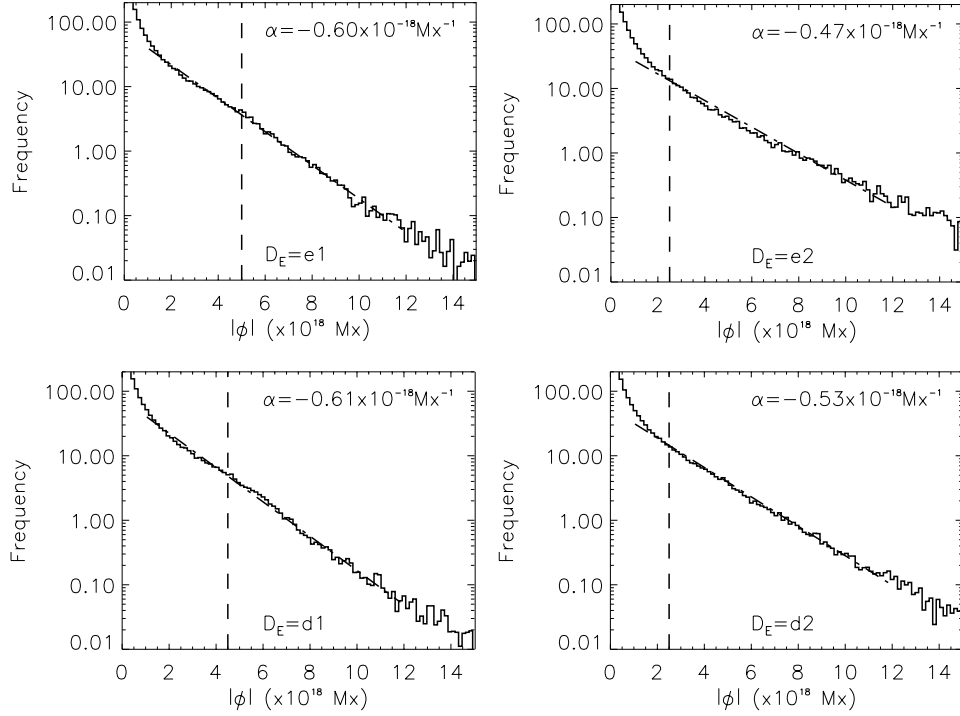


Figure 10. Plots of the number density of concentrations against concentration flux for runs with an emergence rate  $R_E = 8.3 \times 10^{-6} \text{ Mx cm}^{-2} \text{ s}^{-1}$  and a fragmentation rate  $R_f = 4.2 \times 10^{-5} \text{ s}^{-1}$ , equivalent to one fragmentation every 400 min. The distribution of the emerged flux,  $D_E$ , varies between each plot and is equal to  $e1$  and  $e2$  in the top pair, and  $d1$  and  $d2$  in the bottom pair. Each plot has been normalized to reflect a single field of view of size  $483''$  by  $297''$  and has a bin size of  $0.5 \times 10^{18} \text{ Mx}$ .

particular set of observations of the quiet Sun has an exponential distribution with index  $-1.0 \times 10^{-18} \text{ Mx}^{-1}$ . This was for a data set that had been normalized to reflect a single field of view of  $483''$  by  $297''$ .

Figure 10 shows four plots of the number density of concentrations of a given flux against flux normalized to reflect a single field of view of size  $483''$  by  $297''$ . In each plot, the flux has an emergence rate,  $R_E$ , of  $8.3 \times 10^{-6} \text{ Mx cm}^{-2} \text{ s}^{-1}$  and a fragmentation rate,  $R_f = 4.2 \times 10^{-5} \text{ s}^{-1}$ , equivalent to one cancellation every 400 min. However, the distribution of the emerged flux,  $D_E$ , varies in each graph; exponential in the top row and skewed-normal in the bottom row. In all the graphs the minimum value of the emerged flux is indicated with a vertical line. Exponential flux distribution profiles are found in all graphs. To the left of the first dashed line, concentrations are produced by the processes of fragmentation and cancellation and to a limited extent by coalescence, whereas to the immediate right of these lines the concentrations are produced by emergence as well. Clearly, in all

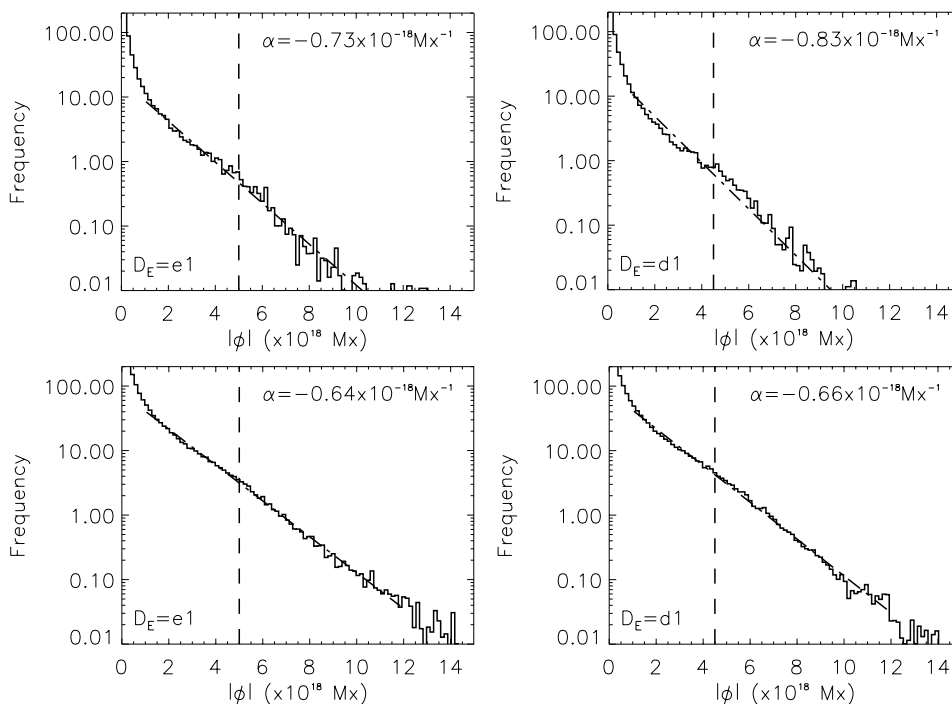


Figure 11. Plots of the number density of concentrations against concentration flux. The top two graphs have an emergence rate  $R_E = 5.0 \times 10^{-6} \text{ Mx cm}^{-2} \text{ s}^{-1}$  and a fragmentation rate  $R_f = 4.2 \times 10^{-5} \text{ s}^{-1}$  equivalent to one fragmentation every 400 min. The bottom two have an emergence rate  $R_E = 8.3 \times 10^{-6} \text{ Mx cm}^{-2} \text{ s}^{-1}$  and a fragmentation rate  $R_f = 1.1 \times 10^{-4} \text{ s}^{-1}$  equivalent to one fragmentation every 200 min. The two graphs on the left have an emergence distribution,  $D_E = e1$ , whilst in the two on the right,  $D_E = d1$ . Each plot has been normalized to reflect a single field of view of size  $483''$  by  $297''$  and has a bin size of  $0.5 \times 10^{18} \text{ Mx}$ .

plots the effect of fragmentation dominates the flux distribution at small scales, as found by Schrijver *et al.* (1997).

The indices,  $\alpha$ , of the exponential distributions in the graphs of Figure 10 have been estimated assuming that the frequency (number density of flux concentrations) and flux,  $|\phi|$ , are related in the following manner:

$$\text{frequency} = Ae^{\alpha|\phi|} . \quad (4)$$

In each case, the best fitting exponential curve determined using a least squares fit is indicated on the plots with a dot-dashed line. The curve is fitted between  $1.0 \times 10^{18} \text{ Mx}$  and  $1.2 \times 10^{19} \text{ Mx}$ . The indices,  $\alpha$  ( $\text{Mx}^{-1}$ ) of these exponentials are shown in each plot.

Clearly, all these indices are shallower than the observed value of  $-1.0 \times 10^{18} \text{ Mx}^{-1}$ . If, for instance, we considered a distribution of concentration fluxes with a lower emergence rate,  $R_E$ , but the same fragmentation rate, then in all cases the exponential indices increase (e.g., Figure 11). If instead, we consider

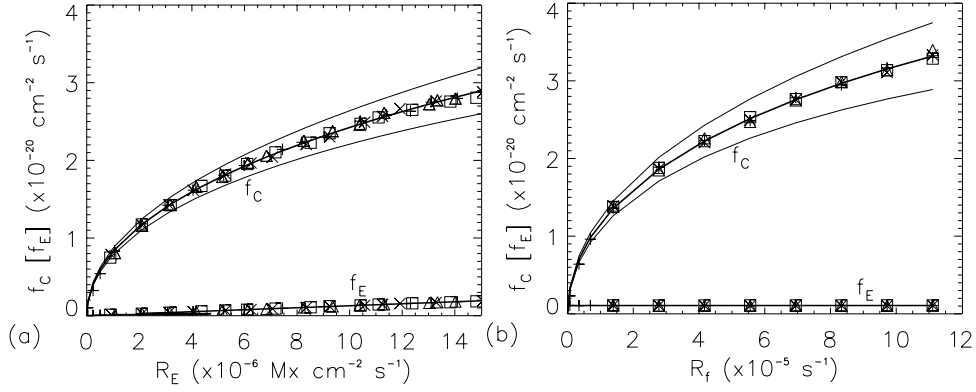


Figure 12. Frequency of cancellation,  $f_C$ , and frequency of emergence,  $f_E$ , versus (a) emergence rate,  $R_E$ , and (b) fragmentation rate,  $R_f$ , for emerged flux distributions,  $D_E$  equal to  $e1$  ( $\Delta$ ),  $e2$  ( $\square$ ),  $d1$  ( $+$ ), and  $d2$  ( $\times$ ). In (a) the fragmentation rate,  $R_f$ , is held fixed at  $4.2 \times 10^{-5} \text{ s}^{-1}$ , which is equivalent to one fragmentation every 400 min and in (b) the emergence rate,  $R_E$ , is held fixed at  $8.3 \times 10^{-6} \text{ Mx cm}^{-2} \text{ s}^{-1}$ . The *solid curves* represent the lines of best fit through the data sets. The *thin curves* enclosing the frequency of cancellation data represent the fits given by twice the standard error.

a distribution of concentration fluxes with the same emergence rate as before, but a higher fragmentation rate, then again, in all cases, the exponential indices increase (e.g., Figure 11).

### 3.3. CANCELLATION

The process of cancellation occurs naturally within the model and is governed by the rules we have set for the movement of the flux concentrations and the number of concentrations that exist. Hence, the rate of cancellation is not an input parameter, but is implicit in the model. We can calculate from the model the rate and frequency of cancellation, as well as the distribution of the canceled flux.

The cancellation rate,  $R_C$  ( $\text{Mx cm}^{-2} \text{ s}^{-1}$ ), is found to be basically identical to the flux emergence rate,  $R_E$  ( $\text{Mx cm}^{-2} \text{ s}^{-1}$ ), for all the emerged flux distributions,  $D_E$ , indicating that the models have been run long enough such that the absolute flux density now oscillates around an equilibrium state (see Figure 7). Indeed, a line of best fit through the data is the line  $R_E = R_C$  with errors on the exponents too small to be significant. This result is reassuring indicating that the rules of motion are reasonable, at least with respect to cancellation, since this is what we believe happens on the Sun. However, it does not tell us much about the numbers of cancellations occurring and the distribution of the canceled flux.

In Figure 12(a) the frequency of cancellation,  $f_C$  ( $\text{cm}^{-2} \text{ s}^{-1}$ ), is plotted against  $R_E$  ( $\text{Mx cm}^{-2} \text{ s}^{-1}$ ) for emerged flux distributions,  $D_E$ , equal to  $e1$  ( $\Delta$ ),  $e2$  ( $\square$ ),  $d1$  ( $+$ ), and  $d2$  ( $\times$ ). Also plotted on this graph is the frequency of emergence,  $f_E$  ( $\text{cm}^{-2} \text{ s}^{-1}$ ), against  $R_E$  ( $\text{Mx cm}^{-2} \text{ s}^{-1}$ ), for all the emerged flux distributions.

The rate of fragmentation,  $R_f$ , is held fixed at  $4.2 \times 10^{-5} \text{ s}^{-1}$ , which is equivalent to one fragmentation every 400 min per concentration. The solid curves represent the best fits through the two data sets. The thin curves enclosing the frequency-of-cancellation data represent the fits given by twice the standard error.

Not surprisingly, the frequency of emergence,  $f_E$ , is linearly dependent on the rate of flux emergence,  $R_E$ . Indeed, assuming the  $f_E = 0$  when  $R_E = 0$ , we find

$$f_E = (1.28 \pm 0.009) \times 10^{-16} R_E . \quad (5)$$

However, the frequency of cancellation,  $f_C$ , has a more complicated dependence on  $R_E$  given by the following relation:

$$f_C = a_0 \sqrt{R_E} + a_1 R_E , \quad (6)$$

where  $a_0 = (8.51 \pm 0.31) \times 10^{-18}$  and  $a_1 = (-2.66 \pm 1.16) \times 10^{-16}$ . Furthermore, the frequency of cancellation,  $f_C$ , is also dependent on the fragmentation rate,  $R_f$ , in a similar way, but here  $a_0 = (3.92 \pm 0.17) \times 10^{-18}$  and  $a_1 = (-7.29 \pm 2.25) \times 10^{-17}$ , as seen in Figure 12(b). The frequency of emergence,  $R_E$ , is independent of the fragmentation rate,  $R_f$ , as one would expect. Note, in all the above equations the errors quoted are twice the standard error.

Obviously, if the rate of cancellation and emergence are almost equivalent, but the frequency of cancellation is much greater, then the amount of flux lost per cancellation must be much less than the amount emerged. In Figure 13, the number density of the canceled flux is plotted against flux for all four emerged flux distributions,  $D_E$ . The emergence rate,  $R_E$ , is kept fixed at  $8.3 \times 10^{-6} \text{ Mx cm}^{-2} \text{ s}^{-1}$  and the rate of fragmentation,  $R_f$ , is also fixed at  $4.2 \times 10^{-5} \text{ s}^{-1}$ . Note, that here the number density of cancellations is estimated by determining the total number of cancellations over the entire simulation and then normalizing to reflect the number per  $\text{cm}^2$  per second. This is different from the approach used to determine the number density of the fragments. In determining the number density of the fragments the same approach as Schrijver *et al.* (1997) was used so that a comparison could be made with the observations. Normalizing the number density to be that in a single field of view of size  $483''$  by  $297''$  leads to a steeper exponential slope being estimated than if the number density of fragments were calculated by the method used for calculating the number density of cancellations.

All four canceled flux distributions are very similar. An exponential curve has been fitted to the data between  $1.0 \times 10^{18} \text{ Mx}$  and  $6.0 \times 10^{18} \text{ Mx}$ , using the least-squares method, and has the form

$$N_C = A_C e^{\alpha_C |\phi_C|} , \quad (7)$$

where  $|\phi_C|$  (Mx) is flux of canceled concentration and the number density of the canceled flux is  $N_C$  ( $\text{Mx}^{-1} \text{ cm}^{-2} \text{ s}^{-1}$ ). The estimates of the exponential indices,  $\alpha_C$ , and the constants,  $A_C$ , are shown on the graphs in Figure 13, with  $A_0 = 1 \text{ Mx}^{-1} \text{ cm}^{-2} \text{ s}^{-1}$ . The results suggest that the emerged flux distribution has

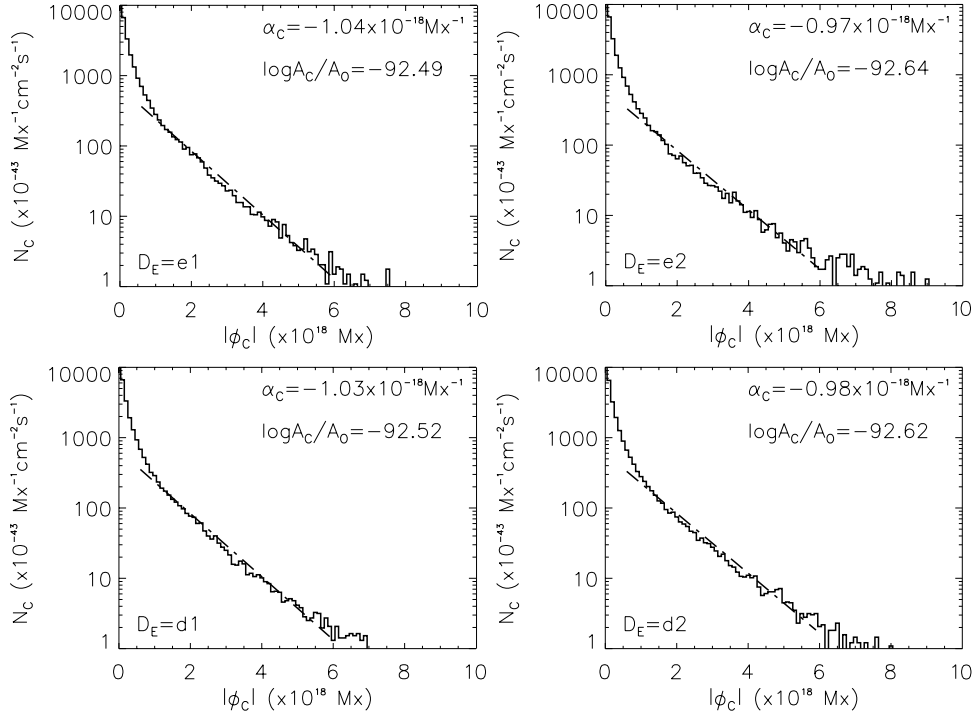


Figure 13. Plots of the number density of canceled concentrations against concentration flux for runs with an emergence rate  $R_E = 8.3 \times 10^{-6} \text{ Mx cm}^{-2} \text{ s}^{-1}$  and a fragmentation rate  $R_f = 4.2 \times 10^{-6} \text{ s}^{-1}$  equivalent to one fragmentation every 400 min per concentration. The distribution of the emerged flux,  $D_E$ , varies between each plot and is equal to  $e1$ ,  $e2$ ,  $d1$ , and  $d2$  going from left to right and from top to bottom across the plots. The *dot-dashed* lines are the lines of best fit used to determine the index of the power law.  $A_0 = 1 \text{ Mx}^{-1} \text{ cm}^{-2} \text{ s}^{-1}$

a greater effect than the fragmentation rate on both the index of the exponential,  $\alpha_C$ , and on the actual numbers of concentrations represented by  $\log A_C/A_0$ .

Clearly, the canceled flux distributions are very different from those for the emerged flux concentrations which are shown in Figure 14, where again the exponential indices,  $\alpha_E$ , are shown on the graphs.

#### 4. Conclusions

A two-dimensional simulation of the quiet-Sun solar magnetic carpet has been developed and is used to investigate the effects of emergence rate,  $R_E$ , and emerged flux distribution,  $D_E$ , and fragmentation rate,  $R_f$ , on the absolute flux density, the flux distribution and cancellation. The fragments in the simulation are moved around according to a series of rules that have been chosen to map as closely as possible the actual movement of fragments on the surface of the quiet Sun. It is found that the total flux density of the system readily relaxes to a state where it

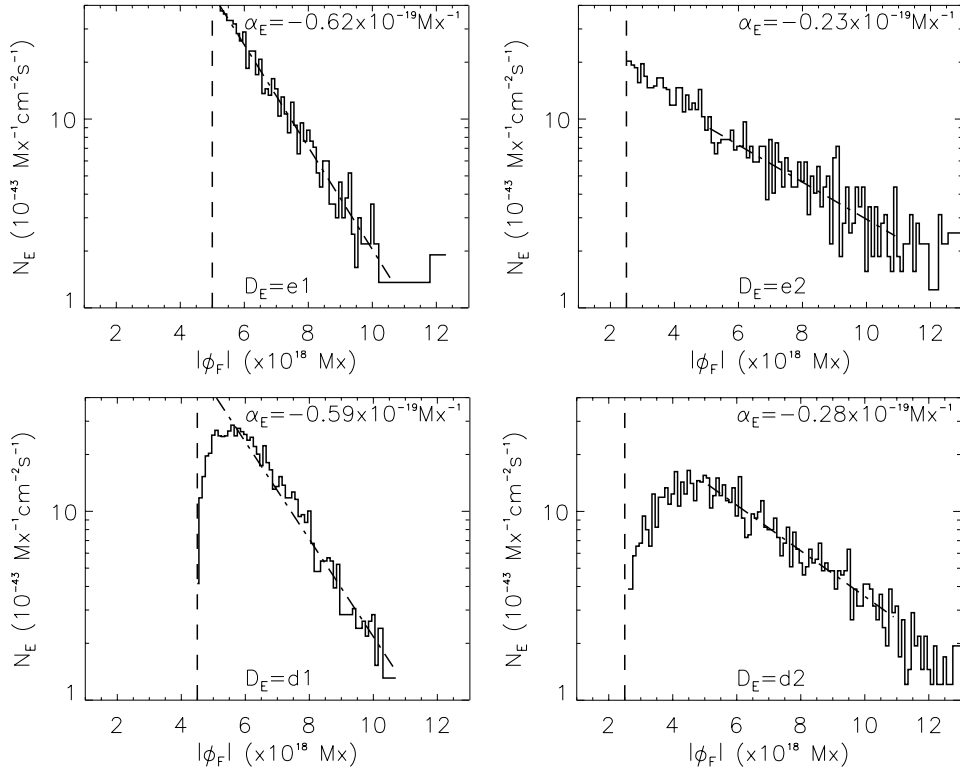


Figure 14. Plots of the number density of emerged concentrations against concentration flux for runs with an emergence rate  $R_E = 8.3 \times 10^{-6} \text{ Mx cm}^{-2} \text{ s}^{-1}$  and a fragmentation rate  $R_f = 4.2 \times 10^{-6} \text{ s}^{-1}$  equivalent to one fragmentation every 400 min per concentration. The distribution of the emerged flux,  $D_E$ , varies between each plot and is equal to  $e1$ ,  $e2$ ,  $d1$  and  $d2$  going from left to right and from top to bottom across the plots. The *dot-dashed lines* are the lines of best fit used to determine the index of the power law and the *dashed lines* indicate the minimum flux in each distribution,  $D_E$ .

oscillates about an average absolute flux density,  $\bar{b}$ . The size of the oscillations can be fairly large,  $\pm 2 \text{ G}$  if  $\bar{b} = 3 \text{ G}$ , but since the rate of cancellation is practically identical to the rate of emergence, we are confident that we have found a steady state. The periods of the oscillations appear to be, from inspection, fairly random lying between 10 days and 40 days.

The parameters that affect the value of the average absolute flux density have been explored. It is found that the rate of flux emergence,  $R_E$ , has the most significant effect on  $\bar{b}$ , with not surprisingly,  $\bar{b}$  increasing for increasing  $R_E$ . Initially, this increase is very dramatic with the  $\bar{b} \sim \sqrt{R_E}$ , but, as  $R_E$  gets larger, it is found that  $\bar{b} \sim R_E$ . The absolute flux density is also dependent on the fragmentation rate. When there is very little fragmentation in the system  $\bar{b}$  is greater than if there is a lot of fragmentation. This is because the more concentrations there are the more frequently cancellations can occur and so the average flux density drops for higher

fragmentation. However,  $\bar{b}$  asymptotes to an average value because increasing the number of cancellations, also increases the number of coalescences and so these two effects eventually cancel each other. The distribution of the emerged flux has virtually no effect on the absolute flux density.

The main aim of the paper was to predict the exact values of  $R_E$ ,  $R_f$  and  $D_E$  needed to produce the observed distribution of flux concentrations. It has, however, proved very difficult to do this. The distribution of flux concentrations is practically independent of the distribution of emerged concentrations, but increases with increasing fragmentation rate,  $R_f$ , and decreasing emergence rate,  $R_E$ . However,  $R_E$  and  $R_f$  cannot be varied in any arbitrary way since we also need to maintain sufficient absolute flux density. In the parameter ranges we considered, we found that an emergence rate between  $6 \times 10^{-6}$  and  $1 \times 10^{-5}$  Mx cm $^{-2}$  s $^{-1}$  and an fragmentation of greater than  $12 \times 10^{-5}$  s $^{-1}$  is the most likely combination to give both the correct absolute flux density and flux distribution.

The rate, frequency and distribution of cancellation were also investigated. It has been found in our simulation that it is not long before the rate of cancellation (Mx cm $^{-2}$  s $^{-1}$ ) equals the emergence rate (Mx cm $^{-2}$  s $^{-1}$ ). However, the frequency of cancellations (cm $^{-2}$  s $^{-1}$ ) is considerably greater than the frequency of emergences (cm $^{-2}$  s $^{-1}$ ) – that is, there are many more cancellation events than emergence events. Indeed, the numbers of cancellation events increase for not only increasing fragmentation rate, but also for increasing emergence rate. In fact, it is likely that there will be an order of magnitude or more cancellations than emergences in the quiet Sun. Clearly, this implies that the amount of flux lost through each cancellation event is likely to be significantly smaller than the amount of flux injected through emergence.

These factors will have an effect on the amount of energy injected into the corona. The results here suggest that there are many very little cancellations occurring everywhere. Each cancellation will release a small amount of energy. The sum of all these cancellation events may supply a significant portion of the energy required to heat the quiet corona. Estimates of the energy and spatial distribution from these cancellations forms the basis of anticipated future work. Furthermore, it is likely that the large fragmentation rate and so large a number of small concentrations will lead to an abundance of energy being injected into the corona through the process of fly-bys or flux braiding. Initial estimates for the energy released in such an event has been made by Galsgaard, Parnell, and Blaizot (2000). Including such a potentially important source in estimates of the magnetic energy budget for the quiet Sun is essential.

### Acknowledgements

I would like to thank C. J. Schrijver, T. Neukirch, E. R. Priest, and K. Harvey for invaluable discussions during the development of the model and the referee, H. J. Hagenaar, for her helpful suggestions for improvements to this paper. I must

thank the Royal Astronomical Society for their support, in the form of the RAS Sir Norman Lockyer Fellowship.

### References

- Galsgaard, K., Parnell, C. E., and Blaizot, J.: 2000, *Astron. Astrophys.* **362**, 395.
- Hagenaar, H. J., Schrijver, C. J., and Title, A. M.: 1997, *Astrophys. J.* **481**, 988.
- Hagenaar, H. J., Schrijver, C. J., Title, A. M., and Shine, R. A.: 1999, *Astrophys. J.* **511**, 932.
- Harvey, K. L.: 1984, *Proc. Fourth European Meeting on Solar Physics, The Hydromagnetics of the Sun*, ESA SP-220, p. 235.
- Harvey, K. L.: 1993, PhD Thesis, Astronomical Institute, Utrecht University.
- Harvey, K. L. and Harvey, J. W.: 1976, in S. F. Martin and K. L. Harvey (eds.), *Part II Air Force Report AFGL-TR-76-0225*, p. 35.
- Harvey, K. L. and Martin, S. F.: 1973, *Solar Phys.* **32**, 389.
- Harvey, J. W., Harvey, K. L., and Martin, S. F.: 1975, *Solar Phys.* **40**, 87.
- Livi, S. H. B., Martin, S. F., and Wang, J.: 1985, *Australian J. Phys.* **38**, 855.
- Livingston, W. C. and Harvey, J. W.: 1975, *Bull. Amer. Astron. Soc.* **7**, 346.
- Martin, S. F.: 1984, in S. L. Keil (ed.), *Proc. Symp. on Small-scale Dynamical Processes in Quiet Stellar Atmospheres*, National Solar Observatory, Sacramento Peak, NM, p. 30.
- Martin, S. F.: 1988, *Solar Phys.* **117**, 243.
- Martin, S. F.: 1990, in J. O. Stenflo (ed.), *Solar Photosphere: Structure, Convection and Magnetic Fields*, Proceedings of the 138th Symposium of International Union, Kiev, U.S.S.R., Kluwer Academic Publishers, Dordrecht, p. 129.
- Martin, S. F. and Harvey K. L.: 1979, *Solar Phys.* **64**, 93.
- Martin, S. F., Livi, S. H. B., and Wang, J.: 1985, *Australian J. Phys.* **38**, 929.
- Martin, S. F., Livi, S. H. B., Wang, J., and Shi, Z.: 1985, in M. Hagyard (ed.), *Proceedings of the Workshop on Vector Magnetic Fields* NASA CP 2374, p. 403.
- Scherrer, P. H., Bogart, R. S., Bush, R. I., Hoeksema, J. T., Kosovichev, A. G., Schou, J., Rosenberg, W., Springer, L., Tarbell, T. D., Title, A., Wolfson, C. J., and Zayer, I.: 1995, *Solar Phys.* **162**, 129.
- Schrijver, C. J. and Harvey, K. L.: 1994, *Solar Phys.* **150**, 1.
- Schrijver, C. J., Title, A. M., van Ballegoijen, A. A., Hagenaar, H. J., and Shine, R. A.: 1997, *Astrophys. J.* **487**, 424.
- Schrijver, C. J. and Zwaan, C.: 2000, *Cambridge Astrophysics Series* **34**, Cambridge University Press, Cambridge.
- Simon, G. W. and Leighton, R. B.: 1964, *Astrophys. J.* **140**, 1120.
- Spruit, H. C., Nordlund, A., and Title, A.: 1990, *ARA&A* **28**, 263.
- Title, A.: 2000, *Phil. Trans. R. Soc. London* **A358**, 657.
- Wang H.: 1988, *Solar Phys.* **117**, 343.
- Wang, H., Tang F., Zirin H., and Wang, J.: 1996, *Solar Phys.* **165**, 223.
- Wang H. and Zirin H.: 1988, *Solar Phys.* **115**, 205.
- Wang H., Zirin H., and Shi, Z.: 1985, *Solar Phys.* **98**, 241.
- Wang, J. and Shi, Z.: 1988, *Acta. Astron. Sinica* **29**, 48.
- Wang, J., Wang, H., Tang F., Lee J. W., and Zirin H.: 1995, *Solar Phys.* **160**, 277.
- Webb, D. F., Martin, S. F., Moses, D., and Harvey, J. W.: 1993, *Solar Phys.* **144**, 15.
- Weiss, N.O.: 1994, in M. R. E. Proctor & A. D. Gilbert (eds.), *Lectures on Solar and Planetary Dynamos*, Cambridge University Press, Cambridge, pp. 59–95.
- Zirin, H.: 1985, *Australian J. Phys.* **38**, 961.
- Zirin, H.: 1987, *Solar Phys.* **110**, 101.
- Zwaan, C.: 1987, *Ann. Rev. Astron. Astrophys.* **25**, 83.